第39卷第6期 无 机 化 学 学 报 Vol.39 No.6
2023年6月 CHINESE JOURNAL OF INORGANIC CHEMISTRY 1193-1207

初始微观结构缺陷和断裂的温度依赖及相关性

赵健伟*,[1] 沈坤燕[2] 于晓辉[1] 侯 进*,[3,4]
([1]嘉兴学院,浙江省纱线材料成形与复合加工技术研究重点实验室,嘉兴 314001)
([2]西南交通大学计算机与人工智能学院,成都 611756)
([3]西南交通大学信息科学与技术学院,智能感知智慧运维实验室,成都 611756)
([4]西南交通大学,综合交通大数据应用技术国家工程实验室,成都 611756)

摘要: 纳米线(NW)结构内的微观结构缺陷对NW的机械性能存在一定的影响。NW断裂位置的预测关系着纳米器件应用的寿命,进而引起了人们的广泛关注。在本工作中,基于统计分析,分别研究了单晶铜纳米线(Cu NW)拉伸过程中出现的断裂位置以及在应力屈服点处产生的初始微观结构缺陷(初始缺陷)的位置对温度的依赖性,进一步探究了两者之间的联系。利用分子动力学(MD)模拟了单晶Cu NW在20~300 K的温度范围内的拉伸状态,共包含6个体系,各温度体系包含300个独立的样本。基于机器学习,采用density-based spatial clustering of applications with noise(DBSCAN)算法,将hexagonal close-packed(*hcp*)原子划分为各个初始缺陷以进一步确定其位置。统计结果显示,当温度低于50 K时,初始缺陷的位置集中在NW的两端。随着模拟温度的上升,MD模拟结果展现了单晶Cu NW的拉伸过程中的杨氏模量、平均屈服应力、平均势能等机械性能对温度的依赖性。温度的升高进一步促使了更多初始缺陷的产生,并使得初始缺陷的位置由统计分布的两端向中间平均化。与初始缺陷相比,各温度下的断裂位置集中在两端。统计结果表明,模拟的温度范围对NW的断裂位置无明显影响,但对初始缺陷的产生具有明显影响。当温度低于100 K时,初始缺陷的位置分布与断裂位置分布呈现了一致性。由于两者具有不同的温度依赖,其差异随着温度的上升逐渐显现。对不同温度下的微观结构形变行为观察发现,断裂失效明显受到NW两端的表面效应和阻挡效应的影响。最终的断裂位置受塑性形变中后期的影响,与应力屈服区产生的初始缺陷无直接联系。

关键词: 纳米线; 初始微观结构缺陷; 断裂失效; 分子动力学; 统计分析; 机械性能
中图分类号: O641 **文献标识码:** A **文章编号:** 1001-4861(2023)06-1193-15
DOI: 10.11862/CJIC.2023.075

Temperature dependence and correlation of initial microstructural defects and breaking

ZHAO Jian-Wei*,[1] SHEN Kun-Yan[2] YU Xiao-Hui[1] HOU Jin*,[3,4]
([1]*Key Laboratory of Yarn Materials Forming and Composite Processing Technology, Jiaxing University, Jiaxing, Zhejiang* 314001, *China*)
([2]*School of Computing and Artificial Intelligence, Southwest Jiaotong University, Chengdu* 611756, *China*)
([3]*Laboratory of Intelligent Perception and Smart Operation & Maintenance, School of Information Science and Technology, Southwest Jiaotong University, Chengdu* 611756, *China*)
([4]*National Engineering Laboratory of Integrated Transportation Big Data Application Technology, Southwest Jiaotong University, Chengdu* 611756, *China*)

Abstract: The microstructural defects within the nanowire (NW) have a significant impact on the mechanical properties of the NW. The prediction of the breaking position of the NW has raised concerns owning to it is a crucial point in the application of nanodevices. In this work, based on the statistical analysis, the breaking positions and the positions of the initial microstructural defects generated at the stress yield point are studied separately to analyze

收稿日期:2022-12-01。收修改稿日期:2023-04-21。
国家自然科学基金国际(地区)合作与交流(No.51861145202)资助。
*通信联系人。E-mail:jwzhao@zjxu.edu.cn,jhou@swjtu.edu.cn

their temperature dependence, then further investigate the relationship between the breaking failure and the initial microstructural defects. At the temperature range from 20 to 300 K, including six ensembles, the single-crystal Cu NWs have been performed using molecular dynamics (MD) simulations. The ensemble at each temperature includes 300 independent samples. Based on machine learning, the hexagonal close-packed (*hcp*) atoms at the stress yield point have been clustered to every initial microstructural defect by the density-based spatial clustering of applications with noise (DBSCAN) algorithm. According to the statistical results, it is found that the initial microstructural defects of NWs simulated in this paper tend to generate at the two ends of the NW while the temperature is less than 50 K. Following the increasing temperature, the MD simulation results have shown a strong temperature dependence of mechanical properties for the single-crystal Cu NWs, including Young′s modulus, average yield stress, average potential energy, etc. It is attributed that there are more initial microstructural defects generated as the increase in temperature, and the positions of initial microstructural defects are averaged out from the two ends of the distribution towards the middle part. The breaking positions for all the simulation temperatures are mainly concentrated on the ends of the NW. The statistical results indicate that this temperature range has little effect on breaking position but a great effect on the initial microstructural defects. It shows a consistency between the initial slip distributions and breaking distributions while the temperature is less than 100 K. However, it has been observed that the differences between them are gradually shown with the increase in temperature due to their different temperature dependents. The microstructural deformation behaviors under different temperatures reveal that the breaking failure is affected by the surface effect and blocking effect of the ends. Based on the results, the final breaking position is correlated to the middle and late stages of the plastic deformation rather than the positions of initial microstructural defects first generated.

Keywords: nanowires; initial microstructural defects; breaking failure; molecular dynamics; statistical analysis; mechanical properties

0 Introduction

Metal nanomaterials, as a new class of materials, have been studied extensively in recent years to explore their specific properties for application[1-4]. Among them, Cu nanowires (NWs) are widely used in composites[5], wearable devices[6], sensors[7], and solar cells[8] due to their low production cost, excellent flexibility, high light transmission, and electrical conductivity[4,9]. To increase the service time of the nano-devices, the basic research on the correlation between initial microstructural defects and breaking failure of Cu NWs is particularly significant.

The externally applied loads to the nanodevices would promote a series of microstructural defects to generate within the structure of nanomaterials, which would have a significant impact on the mechanical properties of the material[10] and have been studied by a series of experimental techniques. For example, Li et al.[11] demonstrated a technique for observing the nucleation of individual dislocations during *in-situ* transmission electron microscopy (TEM) tensile testing. Wang et al.[12] observed the sliding of the grain boundaries in *in-situ* atomic-resolution TEM experiments, contributing to understanding interface-mediated deformation and failure mechanisms in polycrystalline materials. However, the capability of experimental methods for large samples and detailed evolution of the microstructure is limited due to complicated surface morphology and the small size of NWs[13-14]. Moreover, the experimental works require advanced techniques, and it usually takes more time and funds but results in fewer samples. In contrast, molecular dynamics (MD) simulation could be a promising method for solving the above problems, which have been widely used in materials science[15-18]. In particular, Cheng et al.[19] simulated the tensile of a series of NWs with different initial structures using MD simulations, finding that the local geometry of nanostructures plays a dominant role in determining the nature and location of mechanical fail-

ure. Moreover, Pang et al.[20] found that the plastic deformation modes transform with the variation of NW orientations by comparing simulated atomic snapshots for different oriented NWs.

On the other hand, with continuous loads applied to the nanomaterials, structural defects will spontaneously occur, leading to a final breaking of the nanodevice. In experiments, fracture behaviors are usually observed in *in-situ* TEM nanomechanical tests[21-22] and scanning electron microscope (SEM) tensile tests[23]. However, the limitation comes from the fact that enormous nanoscale samples would not provide by conventional experiment techniques. In addition, the conventional experimental methods are hard to perform precisely temperature-dependent[24]. Therefore, in our previous works, the MD simulations were used to simulate the tensile of a large number of samples to study the statistical results of fracture positions, indicating the dependence of fracture mechanism on the temperature[25], cross-section[26], and strain rate[27].

Based on these works, a study on the effect of microstructural defects generated at the early stage of plastic deformation on the breaking failure is required, which is beneficial for structural strengthening and repair as well as optimizing design principles. As Yi et al.[28] reported, the emission of the unclosed shear loop plays a crucial role in not only the tensile deformation but also the fracture process of NWs. In our previous work[29], for the tensile of single crystal Cu NWs under an extreme temperature of 10 K, an apparent correlation between the initial microstructural defects and breaking failure has been shown based on the statistical distribution. By considering the investigation for mechanical properties of metal NWs under a low-temperature range conducive to application, such as the low-temperature wearable strain sensors[30], two following aspects need to be discussed in detail. Firstly, one would answer the question of how the temperature affects the distribution features of initial microstructural defects and breaking failure. Secondly, it is essential to know the relationship between the initial microstructural and breaking failure at a temperature range based on the statistical analysis.

The direct observation of the deformation mechanism and statistic feature would help us to answer the above two questions. Therefore, in this work, as shown in Scheme 1, the temperature is set as a variable, and the tensile MD simulations of a series of single-crystal Cu NWs with different initial thermal states have been performed to carry out the statistical analysis of initial microstructural defects and breaking failure. Besides, a series of properties and microstructural deformation

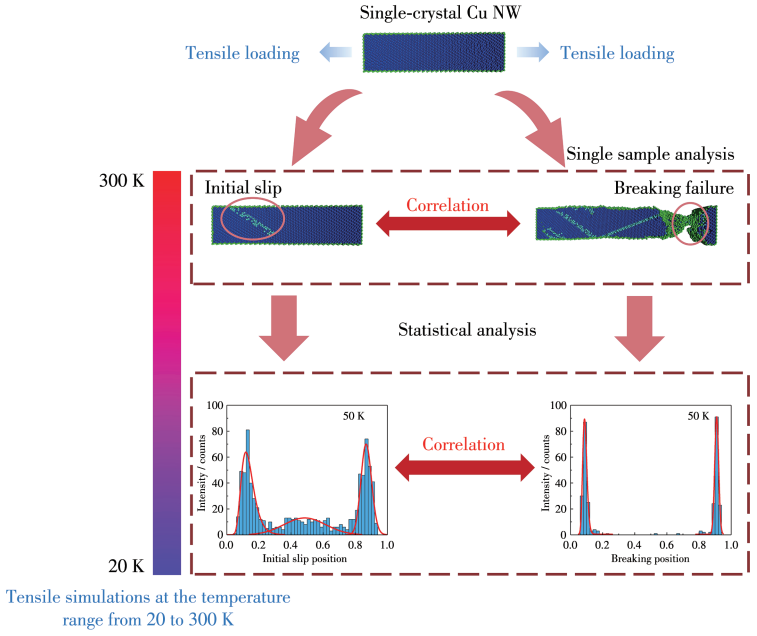

Scheme 1　Schematic explanation of this research

behaviors also have been studied in detail to give a comprehensive understanding, which is contributing to promoting the fundamental research for the prediction of breaking failure.

1 Methodology

1.1 Molecular dynamics simulation

The single-crystal Cu NWs with face-centered cubic (*fcc*) lattice along [111] orientation have been modeled for this study, in which with a dimension of 6.25 nm×5.23 nm×19.17 nm. To study the relationship between initial microstructural defect and breaking failure at different temperatures, the temperatures of six ensembles have been set from 20 to 300 K, and all the tensile simulations were performed with a constant strain rate of $0.1\%\cdot ps^{-1}$, corresponding to an absolute speed of 19.1 $m\cdot s^{-1}$ along the axial direction. Before applying the tensile loads, the free relaxation for an average relaxation time of *ca*. 10 000 MD steps was carried out by each sample to reach an equilibrium state[27]. Following thermal equilibration, the relaxation time for each sample increased by 50 MD steps to ensure the randomness and independence in samples. The ensemble corresponding to each temperature included 300 samples with the same initial atomic arrangement but different initial states, which were characterized by the different thermal movements of atoms. The tensile stress loading along the axial direction was applied by the fixed layers which are set by every four atoms layer at the ends of the NW. In this work, the embedded-atom method (EAM) potential[31] has been used to describe the interatomic interactions which are expressed as

$$E = \frac{1}{2}\sum_{ij} V(r_{ij}) + \sum_i F(\rho_i) \quad (1)$$

$$\rho_i = \sum_{j\neq i} \phi(r_{ij}) \quad (2)$$

where E is the total potential energy of the system, $V(r_{ij})$ is the pair potential energy between atoms i and j, and r_{ij} is the distance between them, $\phi(r_{ij})$ is the electron density at atom i due to atom j as a function of distance r_{ij}, ρ_i is the electron density at atom i due to all other atoms, $F(\rho_i)$ is the energy to embed atom i in an electron density ρ_i. The parameters of EAM potential for Cu used in this paper were referred to as that developed by Johnson[32-33], which have been widely used in published works[34-35].

The tensile loading was simulated using the self-developed software NanoMD[36], in which the free boundary condition was used to simulate the working condition of the NW structure. The Verlet and Cell-linked list[37] was performed to build the adjacent list. The Leap-Frog[38] algorithm with an MD step of 2.5 fs was adopted to solve Newton′s equations of motion. During the stretching of the NW, the types and coordinates of atoms, stress, strain, and energy in the NW system have been recorded every 500 MD steps for further analysis.

1.2 Data analysis

The average stress within the NW in the z-direction has been calculated using the virial scheme[39], in which the atomic stress is expressed by the EAM potential function as

$$\sigma_i^{zz} = \frac{1}{\Omega_i}\left\{-m_i(v_i^z)^2 + \frac{1}{2}\sum_{j\neq i}\left[\frac{\partial\varphi}{\partial r_{ij}} + \left(\frac{\partial F}{\partial\rho_i} + \frac{\partial F}{\partial\rho_j}\right)\frac{\partial f}{\partial r_{ij}}\right]\frac{(r_{ij}^z)^2}{r_{ij}}\right\} \quad (3)$$

where σ_i^{zz} is the atomic stress tensor of the atom i in the zz direction (tensile direction), r_{ij}^z is the distance between the atoms i and j in the zz direction, Ω_i and m_i are the volume and mass of the atom i, and v_i^z is the velocity component in the z-direction of the atom i. The parameters of φ, F, ρ, and f in the above equation are from the EAM potential[40]. The strain ε and strain rate $\dot{\varepsilon}$ (the strain per unit time) of the tensile are defined as

$$\varepsilon = \frac{l - l_0}{l_0} \quad (4)$$

$$\dot{\varepsilon} = \frac{\mathrm{d}\varepsilon}{\mathrm{d}t} \quad (5)$$

where l is the actual length of the NW in the z-direction during stretching, l_0 is the length after free relaxation but before stretching, and t is the time.

For the analysis of the crystal structure, the radial distribution function (RDF) has been used to identify the crystal order, in which the $g(r)$ function is defined as

$$g(r) = \frac{2U}{N_m}\left\langle\sum_{i<j}(r - r_{ij})\right\rangle \quad (6)$$

where U is the system volume and N_m is the number of

atoms. The detailed calculation procedures have referred to in the reference report[41].

The study of the relationship between the breaking failure and initial microstructural defects is depended on positions among them. The breaking position of the NW has been calculated using the atom number ratio (ANR)[26], which is defined as follows

$$\mathrm{ANR} = \frac{N_{\mathrm{bottom}}}{N_{\mathrm{total}}} \tag{7}$$

Where N_{bottom} is the atom number in the bottom part after breaking and N_{total} is the total atoms number of the NW.

The initial microstructural defects are referred to as the slips generated at the stress yield point (YP), called initial slips. To get the position of the initial slip, the centrosymmetric parameter (CSP)[42] has been used to obtain all hcp atoms of the NW at the stress YP. The CSP value of each atom is defined as follows

$$p = \frac{1}{D_0^2} \sum_{i=1,6} \left| \boldsymbol{R}_i + \boldsymbol{R}_{i+6} \right|^2 \tag{8}$$

Where $\boldsymbol{R}_i$ and $\boldsymbol{R}_{i+6}$ are the vectors corresponding to the six pairs of opposite nearest neighbors in the *fcc* lattice, and D_0 is the distance of the nearest neighbors. The CSP value of an atom i is defined as the p_i. For reference, $p_i < 0.4$ represents the fcc atoms, $0.7 < p_i < 1.1$ stands for stacking faults, corresponding to the hcp atoms; $p_i > 2.0$ corresponds to the surface atoms of the NWs[29].

Following all *hcp* atoms of the NW at stress YP are obtained, based on the coordinates of these atoms, then cluster all the *hcp* atoms into every slip to get the positions. Considering the initial slips are various in shape and size, and the number of initial slips for each sample is random, the density-based spatial clustering of applications with noise (DBSCAN) algorithm[43] has been used to cluster closely-linked *hcp* atoms into one slip plane. There is no need for giving the clustering numbers beforehand. However, the parameters (e, M) are requisite, which describe the compactness within a group of neighborhoods, where e is the neighborhood distance threshold for a particular *hcp* atom and M is the minimum number of atoms within a neighborhood of this particular *hcp* atom[29]. In this paper, the e was set as 0.08, and the M was set as 8. After the clustering, the coordinate z of every initial slip plane intersected with the lateral edge of the NW is defined as the initial slip position. This method was applied to the analysis of initial slips at the temperature range from 20 to 300 K, however, it provides an element of uncertainty for the analysis of initial slips under a higher temperature than 300 K because of the thermal movement. The positions of initial slips and breaking failure were based on the normalized length of the NW at the stress YP and when it breaks, respectively.

2 Results and discussion

2.1 Temperature dependence of the distributions of initial slip positions

While the tensile stress applied to the NW system is exceeded the ability to resist plastic deformation, a series of microstructural defects such as slip planes are formed in the NW. Generally, the dislocation first occurs at 4/5 of yield stress, which refers to the true YP. With continuous tensile loading, the movement of dislocations promotes the forming of slip planes. When the stress reaches the maximum (YP), the deformed structure shows several {111} slip planes which refer to the initial slips discussed in this work. Fig.1 shows the initial slips of three representative samples at the stress YP. It could be found that these initial slips are usually generated from the sides of the NWs and developed upwards or downwards at an angle to the surface[10]. The published works[44-45] have demonstrated that the physical and mechanical properties of NWs are strongly affected by surface effects and nanosize effects. Therefore, in this paper, the free boundary condition was used to simulate the NW structures. In Fig.1a, two initial slips are generated at the ends of the NW. Moreover, three initial slips in Fig.1b are generated at both the two ends and the middle part of the NW. In Fig.1c, it is seen that several initial slips are generated near the middle part of the NW, indicating that the fixed-end effect on initial microstructure defects is reduced as much as possible even though the tensile load is applied by the two fixed ends. Moreover, the results demonstrate that the number of initial slips gen-

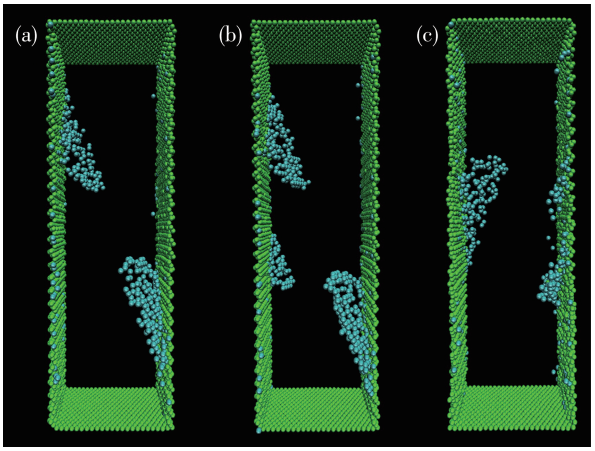

Fig.1 Initial slips generated at the stress YP at (a) 20, (b) 50, and (c) 150 K

erated is random and the positions of initial slips generated could be any part of the NW.

By considering the above representative characteristics of initial slips, the DBSCAN algorithm was used to calculate the normalized position of initial slips. Based on the MD simulations, the normalized positions of initial slips at different temperatures from 20 to 300 K have been analyzed to further investigate the temperature dependence of initial microstructural defects, as shown in Fig. 2. The ratio between the statistical number of initial slips (N_{slips}) and the total number of samples ($N_{samples}$) for each temperature ensemble is defined as

$$\varphi = \frac{N_{slips}}{N_{samples}} \quad (9)$$

The φ under these six temperatures are 2.77, 2.80, 3.36, 3.87, 3.85, and 3.92, respectively. It means that the statistical number of initial slips for each distribution is much more than 300 samples, which is usually 2-4 times the number of samples during this temperature range, and the number of initial slips increases in the temperature range from 20 to 150 K. From 150 to 300 K, the φ fluctuates around 3.88 with its existing statistical errors. In Fig.2a and 2b, it can be observed that high statistical peaks are formed at the ends of distributions, appearing skewed distributions at two ends under the temperatures of 20 and 50 K. Comparatively, the initial slips generated in the interval of 0.2 to 0.8 are not forming the statistical peaks, but following a uniform distribution. It infers the fact that the initial slips of the NWs simulated in this paper tend to generate at the two ends while the temperature is less than 50 K. Under the temperature of 100 K (Fig.2c), there is a tendency of equalization toward the peaks at the ends to the middle part. While the temperature increases to 150 K (Fig.2d), the peak at the left end is almost disappeared, and the peak at the right end significantly

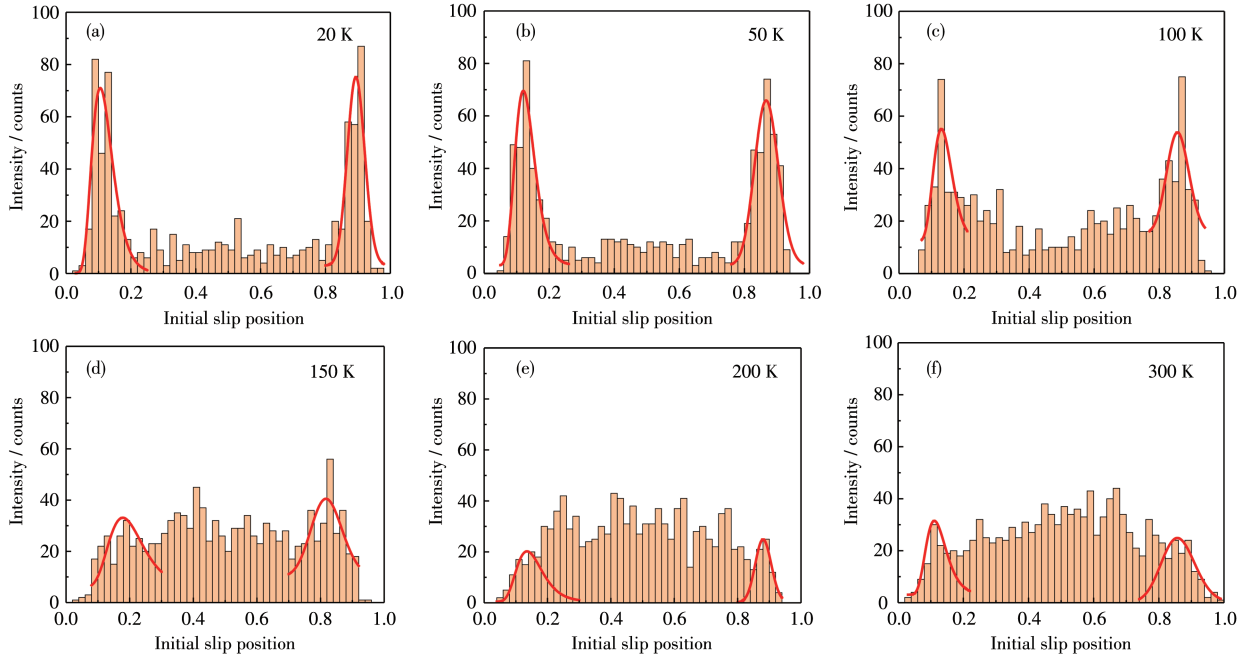

Fig.2 Distributions of initial slip positions for 300 independent samples at different temperatures

decreases with which the height approaching the middle part. At the higher temperatures of 200 and 300 K (Fig.2e, 2f), the positions of initial slips are concentrated on the middle part of the NW rather than the ends. The ratio (θ) of the average peak values at the ends (C_{ends}) and corresponding average counts in the interval of 0.2 to 0.8 (C_{center}) is defined as

$$\theta = \frac{C_{\text{ends}}}{C_{\text{center}}} \tag{10}$$

The θ at the temperatures of 20, 50, 100, 150, 200, and 300 K are 8.14, 7.56, 3.15, 1.34, 0.74, and 0.94, respectively. At temperatures of 200 and 300 K, the θ is less than 1, demonstrating that the generation of initial slips at the ends is restrained at high temperatures. The temperature dependence of peak values is much larger than the fixed-end effect, in which the fixed-end effect is reduced as much as possible in MD simulations. As is well-recognized, thermal motion is related to the change of temperature, leading to the micro atomic fluctuation ways and movements being different[25]. As the above analysis, these microscopic structural changes are also shown statistically in initial slip distributions. Furthermore, a detailed analysis of mechanical properties is necessary to understand how temperature affects the generation and propagation of initial microstructural defects.

2.2 Mechanical properties

The effect of temperature on the deformation mechanism is attributed to the effect on the mechanical properties[10,46]. To further investigate the temperature dependence of the initial slip distribution and deformation mechanism, the correlative properties of the system have been studied.

Fig.3a illustrates how the temperature affects the stress-strain curves of six representative samples. While the stress increases to the maximum value, it is referred to as the stress YP. Generally, the deformation before the YP is referred to as elastic deformation, which is labeled in Fig.3a as region E. At the YP, as above mentioned, the initial slips have been developed sufficiently, promoting the stress to release during the plastic deformation. The plastic deformation corresponds to different deformation states: stress release region, high-stress fluctuation region, and low-stress fluctuation region, which are called regions R, HS, and LS, respectively.

Comparing all stress-strain curves, due to the induced atomic vibrations at elevated temperatures, the fluctuations in these curves increase with the increasing temperature[47]. In region E, the slopes of the stress-strain curves are reflected Young′s modulus of the NWs. The statistical average Young′s modulus (Fig.S1, Supporting information) for each temperature was calculated, and it is found that Young′s modulus decreases with the increase in temperature[10,25,47], which infers that the stiffness of the NW structure is weakened with the increasing of the temperature. Fig. 3b marks the average yield stress and average yield strain, showing a deviation from each sample. As shown in Table 1, with temperature increases, the average yield stress decreases. It is further observed that the mechanical strength of the metallic material reduces with an increase in

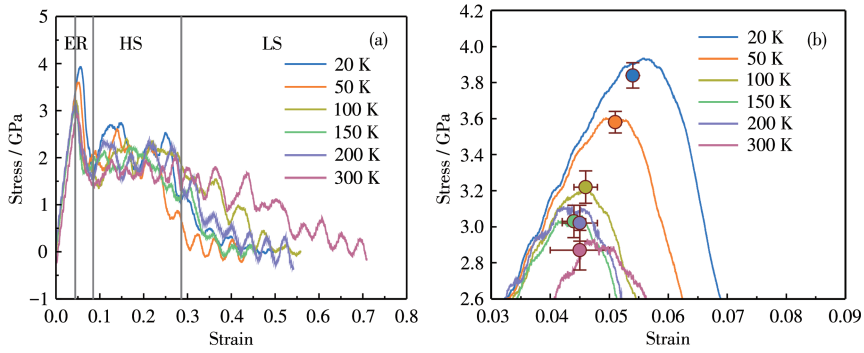

Fig.3　Stress-strain curves of the Cu NW at different temperatures with a constant strain rate of 0.1% ps^{-1}: (a) stress-strain curves of representative samples; (b) average yield stress with error bars for every 300 samples

temperature. From 20 to 100 K, an abrupt decrease is identified and the average yield strains are 0.054 (20 K) and 0.046 (100 K) respectively. From 100 to 300 K, it is found that the average yield strain keeps almost constant with an increase in the temperature. A similar temperature dependence of the yield strain has also been observed in the study of breaking behaviors of the Cu NWs with the dependence of temperature, as Wang et al.[25] reported, the first yield strain almost keeps constant at the temperature range from 100 to 600 K, whereas, the higher temperature (700 K) leads to significant changes in yield strain. At low temperatures, the bigger yield strain and bigger yield stress demonstrate that the stage of elastic deformation is longer. Whereas, the smaller yield stress and smaller Young′s modulus infers that the mechanical strength of the NW reduces at high temperatures, resulting that the yield strain being smaller and keeping almost constant in the temperature range from 100 to 300 K. Such change in the YP demonstrates that the structural change of the NW at different temperatures, especially for the fluctuation of the position and the number of the initial microstructural defect. After the YP, further plastic deformation forces the stress of each system to decrease abruptly in region R and then follows a continuous process of increasing and then decreasing in HS. In the region HS, the stress curves both fluctuated around 2 GPa. However, what is significantly different is that the increase in stress is greater at lower temperatures and the stress tends to decrease as the temperature increases, reflecting the positive effect of higher temperatures on viscoelastic properties. According to that illustrated above, the changes in distributions of initial slips are likely caused by the influence of temperature on the variation in properties of the NW structure. In our previous work[48], it is reported that the generation and development of initial slips are closely related to yielding behaviors. To understand the variation in initial slips more clearly than is possible, more properties of these samples have been analyzed.

Fig.4a shows the energy-strain curves under different temperatures. The average potential energy of the NW increases with the increase in temperature, which is caused by the atomic movement overcoming the interatomic cohesive energy in the tensile deformation process of the NW. At a higher temperature, the average kinetic energy of the atoms increases due to the thermal motion[14], making the atoms more likely to move relative to each other, leading to a significant reduction in the interaction forces and bond strengths between the atoms[46]. Therefore, the average yield stress (Fig.3b) decreases with the increase in temperature. Another important point, it is well-known that the relationship between the average potential energy and temperature is also reflected by the influence of temperature on the degree of lattice order. To clarify

Table 1 Average yield strain and average yield stress for 300 samples at different temperatures

Parameter	20 K	50 K	100 K	150 K	200 K	300 K
Average yield strain	0.054±0.001	0.051±0.001	0.046±0.002	0.044±0.002	0.045+0.003	0.045±0.005
Average yield stress	3.84±0.07	3.58±0.06	3.22±0.09	3.03±0.09	3.02±0.1	2.87±0.11

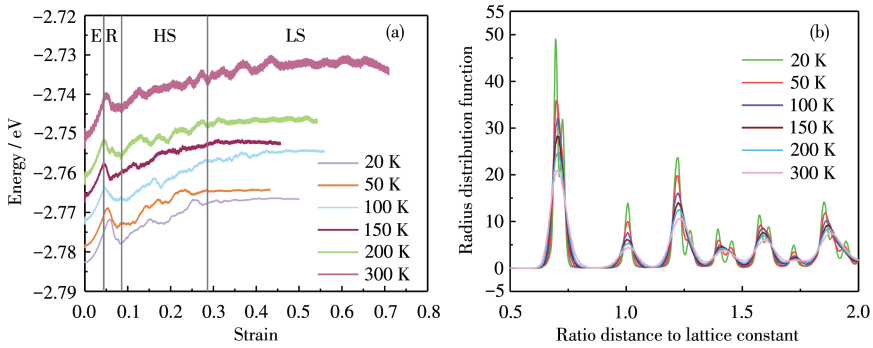

Fig.4 Energy-strain curves during stretching and the curves of RDF: (a) variation of the energy of representative samples with the strain at different temperatures; (b) RDF curves of representative samples at different temperatures

the influence of temperature on the potential energy more clearly to further investigate the structural changes at the YP, Fig.4b shows the RDF at the stress YP for these six samples. At a low temperature of 20 K, the peak value of the RDF curve is very high and sharp, indicating a well-ordered crystalline structure of the Cu NW. With increasing temperature, the peak values of RDF curves gradually decrease and the width increase, which demonstrates that the number of ordered crystal structures decreases with temperature and that of amorphous structures increases[49]. Under a higher temperature, there is a larger magnitude of atomic oscillation, contributing to the atoms overcoming the interatomic cohesive energy to form a disordered amorphous structure, which further induces the increase of the average potential energy[25]. In general, with the temperature increasing, the increases in the average kinetic energy of the atoms and the generation of disordered crystalline structures have collectively resulted in the reduction in the ability to resist plastic deformation of the NW. It means that the initial slips are easier to generate within the NW. Therefore, the average yield strain (Fig.3b) decreases as well as the total number of initial slips increases with the increase of the temperature.

The above analysis has demonstrated the temperature dependence of mechanical properties and yield behaviors, resulting in the changing of the initial slip distribution. At a lower temperature, the yield stress and Young′s modulus in the NW system are higher, showing the brittleness of the NW. As the increasing of the temperature, the decreasing yield stress and Young′s modulus, lead to a reduction in the bonding force within the system. Therefore, the brittleness of the NW is diminished. Accordingly, it shows a positive effect on the ductility of the NW, which leads to more initial slips tending to generate at a lower yield strain. Moreover, it has suppressed the generation of initial slip at both ends. Thus, in the distributions of initial slips under the temperatures from 20 to 300 K (Fig.2a-2f), the peak values at two ends gradually decrease and average out towards the middle part.

To further study the generation and development of initial slips, the variation of the numbers of *hcp* atoms and *fcc* atoms in the tension process has been analyzed, as shown in Fig.5. As the average yield strain of samples decreases with the increase in temperature (Fig.3b), it could be seen that the strains of samples at which the number of the hcp atoms begin to increase are different in Fig.5. After the yield stress, the number of the *hcp* atoms for each sample both linearly increases, correspondingly, the number of *fcc* atoms decreases, which demonstrates the sign of generation of initial slips. Furthermore, the first peak values of the number of *hcp* atoms for these samples are significantly different. Compared with the sample at the temperature of 150 K, the numbers of hcp atoms for others samples continuously increase. It further indicates that the total area of initial slips or the number of initial slips within the system is different from each other (Fig.1)[48].

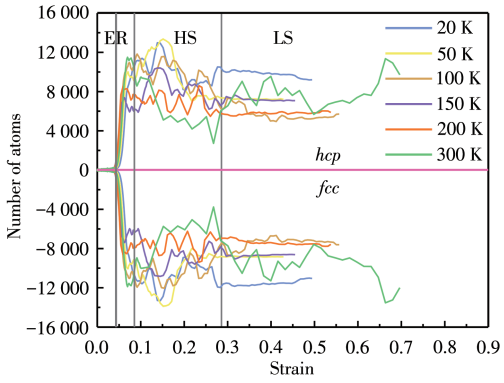

Fig.5　Variation of the number of *hcp* and *fcc* atoms with the strain

The above analysis has shown the effect of temperature on the mechanical properties of the Cu NWs, which was also reported by a series of published studies[20,25,46]. Particularly, it needs to be pointed out the temperature dependence of the initial slips. With further increase in temperature, on the one hand, the positive effect on the ductility of the NW promotes the initial slips generating at a smaller strain to release the stress in the system. On the other hand, it contributes to the changing of initial slip positions from two ends to the middle part of the NW.

2.3　Temperature effect on breaking failure behaviors

With continuous plastic deformation, the NW materials would finally fracture and become useless. If

the breaking position is predictable, the NW could be strengthened timely to avoid fracture failure[50]. Likewise, it significantly contributes to optimizing design principles in manufacturing. Given that the breaking behavior of a single NW sample is not enough to demonstrate the most probable breaking position, the breaking cases of plenty of samples are essential for showing a result of statistical physical chemistry.

In this work, the breaking positions of 300 samples for each simulated temperature ensemble from 20 to 300 K have been counted, as shown in Fig. 6. At each temperature, the characteristics of breaking distribution are similar, which follows two high but asymmetric peaks at two ends. Similarly, Cheng et al.[19] reported that the Cu NWs at the temperature of 10 K tend to break at two ends of the NW, in which the simulated strain rate is similar to this work. In addition, as Liu et al. [50] investigated the effect of the length on the breaking behavior of the Cu NW, the NWs underwent a high-rate stretching with a constant temperature of 300 K, and it was found that as the length of the NW increases, the breaking position gradually shifts to the ends. As above mentioned, it is inferred that the breaking positions of the Cu NWs in present simulated conditions tend to form at two ends of the NW. To give insight into the breaking behavior, it is necessary to understand the properties of the Cu NWs.

In general, the simulation conditions, such as temperature and strain rate, are essential for investigating the deformation behaviors and mechanical properties of the metal NW[25,47]. It is known that the melting temperature of copper is about 1 350 K[51]. However, the maximum temperature simulated is 300 K which is below room temperature and less than a quarter of the melting temperature. Therefore, in this simulated condition, it still shows the brittleness of the Cu NW. Moreover, at this lower range of temperature, there is strong symmetric mechanical impact strength within the ends of the NW, so the stretching shock waves had still not propagated repeatedly through the whole NW, while the NW was already showing the sign of fracture failure at the ends. Thus, the strengthening of the ductility is negligible, the NW simulated in this temperature ranging is still tended to break at the ends.

On the other hand, although the breaking positions of quite a few samples follow distributions at two ends, noted that the number of the discrete samples which break near the middle part of the NW increases with the increase in temperature. Compared with NWs that break at two ends, these discrete samples have better ductility, in which the breaking failure is forming in a larger strain range. Fig. 7 illustrates the average

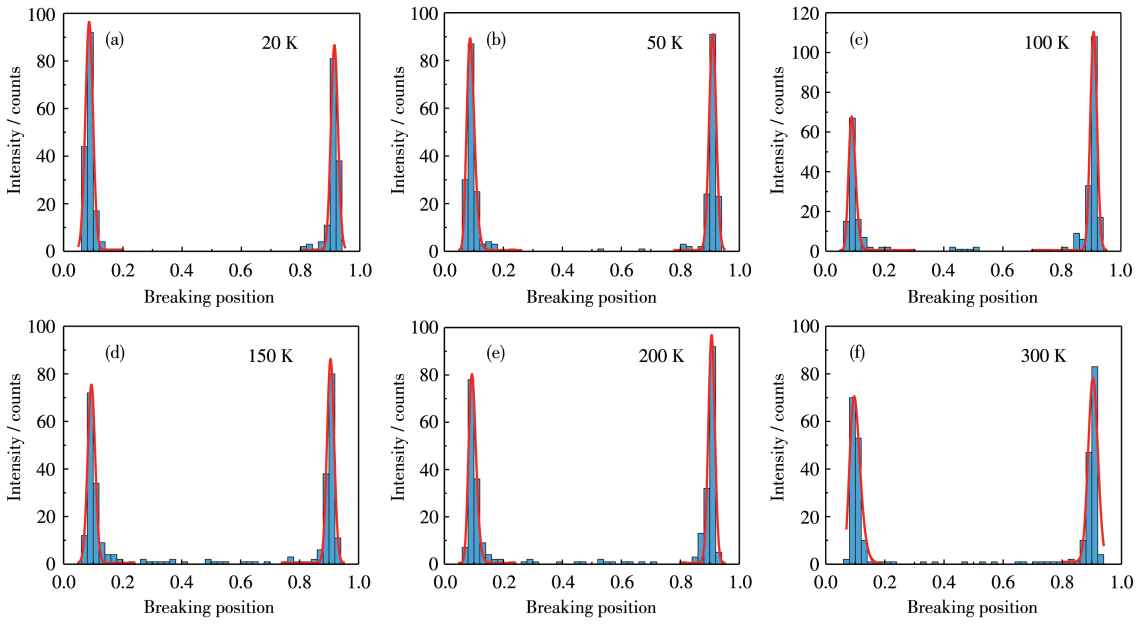

Fig.6 Distributions of breaking positions for 300 samples at different temperatures

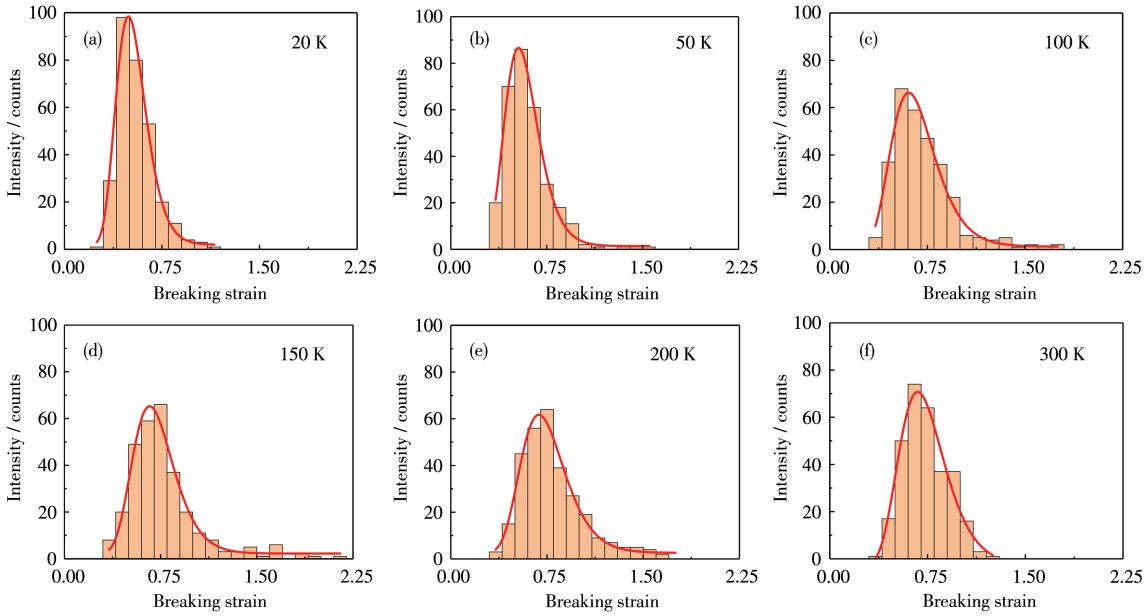

Fig.7　Distributions of average breaking strain for 300 samples at different temperatures

breaking strains of 300 samples under different temperatures, which follow the skewed distributions. At the lower temperatures of 20 and 50 K (Fig.7a, 7b), for the average breaking strains, only a few samples are greater than 1.0. While the temperature increases to 100 K (Fig.7c), the number of samples whose breaking strain is greater than 1.0. The results demonstrate that the increase in temperature promotes the ductility of a few samples, however, the structure of the Cu NW is brittle, leading to the breaking positions at the temperature range from 20 to 300 K both following two statistical peaks at the ends of distributions.

2.4　Relationship between initial microstructural defects and breaking failure

While initial slips are generated in the NW system, it means the beginning of the plastic deformation, and then the further plastic deformation would make the NW break. If the breaking position could be predictable from the initial microstructural defects, it is beneficial for increasing the service life of the materials. However, few works reported whether there is a relationship between the breaking failure and initial microstructural defects. To get a result of statistical analysis to further investigate the relationship between them, in this work, the breaking position distributions and initial slip position distributions under the temperature range from 20 to 300 K have been analyzed as above mentioned. It is found that there are both two obvious statistical peaks in the initial slip distributions and breaking distributions at temperatures of 20, 50, and 100 K, respectively, inferring that there may exist a statistical correlation between them. It means that the initial microstructural defects are tended to generate near two ends of the NW, further leading to most of the samples being broken at two ends. Whereas, with further increase in temperature, the consistency of distribution characteristics among them gradually disappeared due to the different temperature dependence of initial microstructural defects and breaking behaviors. On the one hand, the increasing temperature has restrained the generation of initial slips at two ends. On the other hand, the single-crystal Cu NW simulated in this paper shows the property of stiffness during the temperature range of 20 to 300 K, so most of the samples still prefer to break at two ends even the temperature increases to 300 K. It indicates the statistical correlation between the initial microstructural defects and breaking behaviors is not well understood. To understand this correlation comprehensively, the microstructural deformation behaviors are studied, which depends on the observation of atomistic configuration with different temperatures during tension, as shown in Fig.8.

It shows the microstructures at the YP, region HS, and region LS.

Fig.8a shows the deformation process of the sample at the temperature of 20 K. At the stress YP (0.058), a group of initial slip planes is generated that is parallel and at an angle to the side edges. Generally, the stress within the NW system is released due to the generation of initial slips, so the stress in Fig.3 decreases abruptly after the YP. While the stress is released during region R, the initial slips have been developed adequately, accompanied by the generation of a series of new slip planes. Thus, there is an increase in the number of *hcp* atoms at the strain from 0.058 to 0.1 in Fig.5. Therefore, it is seen that many slips are intersected in the region HS. At the early stage of region HS (0.1 strain), noted that one of the initial slips has propagated to the top of the NW and reflected, following the intersecting with other slips. Further increasing strain, although several slips are intersecting at the bottom of the NW, however, the molten cluster is forming near the top of the NW at the strain of 0.2 which shows up as a stress concentration in the macroscopic view. At the last of region HS, it shows the local melting in the NW, resulting in the necking region and final fracture failure at the top of the NW in region LS. It infers that the breaking failure is related to the propagation of initial slips.

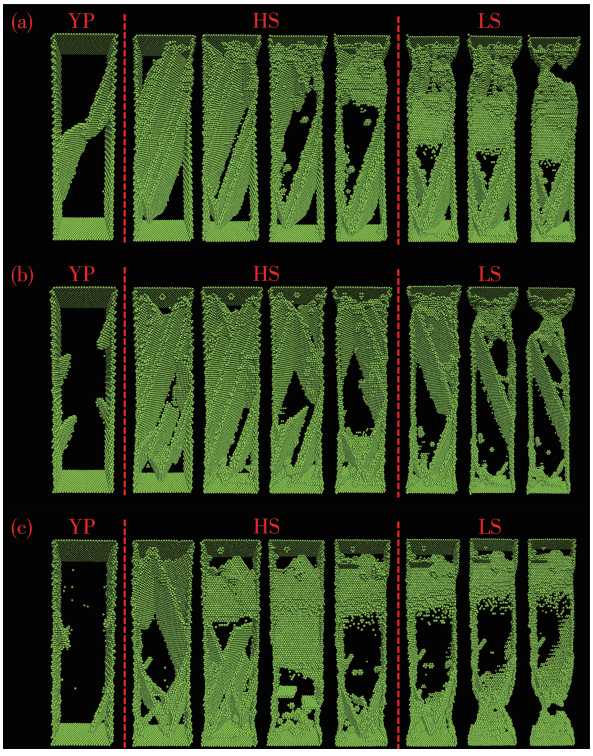

Fig.8 Snapshots of the deformed microstructure with the temperatures of 20, 100, and 200 K at different applied strains: (a) strains in the order of 0.058, 0.1, 0.15, 0.20, 0.25, 0.30, 0.31, 0.40; (b) strains in the order of 0.046, 0.10, 0.15, 0.20, 0.25, 0.30, 0.40, 0.48; (c) strains in the order of 0.042, 0.10, 0.15, 0.20, 0.25, 0.30, 0.40, 0.478

The deformation behavior of the sample in Fig.8b under the temperature of 100 K is similar to that in Fig. 8a. At the YP (0.046 strain), there are two slip planes generated on the left and right sides of the NW, respectively. At the 0.1 strain (region HS), the two initial slips on the left side quickly propagate to the top of the NW and intersect. With further stretching, it is observed that the initial slips on the left and right sides intersect with each other near the top of the NW at 0.2 strain. Finally, for the deformation in region LS, most atoms are irregularly arranged and local atomic dislocations result in atomic stacking and the final necking region. Similarly, as shown in Fig.8c, the initial slips propagate to the bottom of the NW in region HS. In addition, a series of slips intersect near the top of the NW. However, the necking is finally forming at the bottom of the NW in the region LS. As a result, the initial slips would be generated anywhere within the NW and propagate with further stretching. According to that illustrated above, it seems that the final necking region is related to the propagating and intersecting of the initial slips, and it always shows in HS. The microstructural deformation of the samples at the temperatures of 50, 150, and 300 K gives a similar result (Fig.S2). It is illustrated that the deformation mechanism in region HS plays a crucial role in breaking failure. To give insight into the deformation mechanism in region HS, the effect of the boundary could be served as a reference to understand the propagation mechanism of slip planes.

In general, nanomaterial structures are with boundaries, which include side boundaries and the boundaries of the ends, and that is why the free boundary condition is used to simulate the single-crystal Cu

NW in this paper rather than the periodic boundary. While the slips propagate to the side of the NW, the side effect promotes slips to reflect and further develop. In this paper, the initial slips are always developed upwards or downwards, so the slips are easier to develop to the ends of the NW, as shown in Scheme 2. While several slips extended to the ends, a series of atoms is disordered due to the blocking effect from the boundaries of the end, resulting in the local melting in the NW structure and further enhancement of plasticity[52]. Finally, the local necking is easier to form here even though the whole NW system is under the same stress. This indicates that the primary cause that most samples are broken at two ends is the blocking effect from the ends. Furthermore, this also infers that the breaking failure is affected by the propagation of initial slips and new slips generated in region HS rather than the positions where they first appeared. As published works reported, the metal NWs fracture through extensive plasticity and ductile necking[52-54]. Furthermore, the breaking failure of the NW is significantly affected by the middle and late stages of plastic deformation[55]. Therefore, there is no direct causal relationship between the fracture and the initial microstructural defects. It just shows the consistency between the initial slip distributions and breaking distributions while the temperature is less than 100 K.

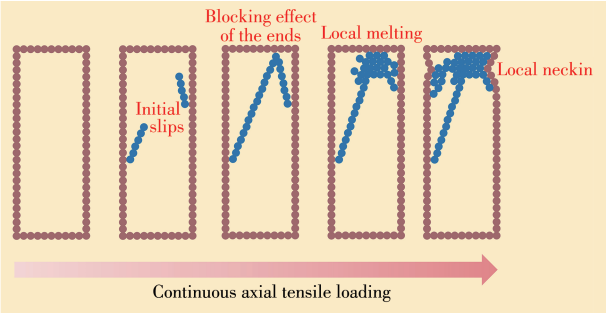

Scheme 2　Schematic explanation of the blocking effect of the ends

3　Conclusions

The study on the effect of microstructural defects generated at the early stage of plastic deformation on the breaking failure is beneficial for structural strengthening and optimizing design principles, which has significant implications for the application of metallic nanomaterials. In this work, based on the statistical analysis, the temperature dependence of the initial microstructural defects (also called initial slips) generated at the stress YP and the temperature dependence of the final breaking positions have been investigated using the MD simulations. At the temperature range of 20 to 300 K, each temperature ensemble includes 300 independent single-crystal Cu NWs. We have calculated the position of the initial slip using the DBSCAN algorithm. Considering the profound significance of predicting the breaking failure of nanostructural materials, we have performed a comprehensive analysis to investigate the relationship between the initial slips and breaking behaviors of the NWs. The results indicate that, with the increase in temperature, the average yield stress decreases due to the decrease in Young′s modulus, the increase in average kinetic energy of atoms, and the increase in amorphous structures, further promoting the average yield strain decreased and more initial slips generated. It is found that the positive effect on the ductility of the NW during the early stage of plastic deformation has restrained the generation of initial slips at two ends. The positions of initial slips are averaged out from the ends toward the middle part of the NW. For the final breaking positions, the structure of the Cu NW is brittle due to the properties of the copper, resulting that the breaking positions under different temperatures are both following two statistical peaks at the ends of distributions. As a result of statistical distributions, it shows a consistency between the initial slip distributions and breaking distributions while the temperature is less than 100 K. However, the consistency between them gradually disappeared with the increase in temperatures because of their different temperature dependence. The microstructural deformation behaviors further demonstrated that there is no direct causal relationship between the fracture and the initial microstructural defects, and the breaking failure is affected by the surface effect and blocking effect of the ends.

Acknowledgments: This work is supported by the National

Natural Science Foundation of China (Grant No.51861145202).

Supporting information is available at http://www.wjhxxb.cn

References:

[1]Francis M K, Sahu B K, Bhargav P B, Balaji C, Ahmed N, Das A, Dhara S. Ag nanowires based SERS substrates with very high enhancement factor. *Phys. E*, **2022**,**137**:115080

[2]Li H L, Ding J W, Cai S F, Zhang W, Zhang X N, Wu T, Wang C, Foss M, Yang R. Plasmon-enhanced photocatalytic properties of Au/ZnO nanowires. *Appl. Surf. Sci.*, **2022**,**583**:152539

[3]Lee J K, Kim B O, Park J, Kim J B, Kang I S, Sim G, Park J H, Jang H I. A bilayer Al nanowire-grid polarizer integrated with an IR-cut filter. *Opt. Mater.*, **2019**,**98**:109409

[4]Yu S H, Liu Z W, Zhao L, Gong B M. High-performance flexible transparent conductive tape based on copper nanowires. *Opt. Mater.*,**2021**, **119**:111301

[5]Yin C G, Liu Z J, Mo R, Fan J C, Shi P H, Xu Q J, Min Y L. Copper nanowires embedded in boron nitride nanosheet-polymer composites with enhanced thermal conductivities for thermal management. *Polymer*, **2020**,**195**:122455

[6]Guo Z G, Sun C, Zhao J, Cai Z S, Ge F Y. Low-voltage electrical heater based on one-step fabrication of conductive Cu nanowire networks for application in wearable device. *Adv. Mater. Interfaces*, **2021**,**8**(3): 2001695

[7]Patella B, Russo R R, O′Riordan A, Aiello G, Sunseri C, Inguanta R. Copper nanowire array as highly selective electrochemical sensor of nitrate ions in water. *Talanta*, **2021**,**221**:121643

[8]Yang J P, Yu F Y, Chen A, Zhao S W, Zhao Y, Zhang S S, Sun T, Hu G Z. Synthesis and application of silver and copper nanowires in high transparent solar cells. *Adv. Powder Mater.*, **2022**,**1**(4):100045

[9]Li D D, Lai W Y, Zhang Y Z, Huang W. Printable transparent conductive films for flexible electronics. *Adv. Mater.*, **2018**,**30**(10):1704738

[10]Xie H X, Yin F X, Yu T, Lu G H, Zhang Y G. A new strain-rate-induced deformation mechanism of Cu nanowire: Transition from dislocation nucleation to phase transformation. *Acta Mater.*, **2015**, **85**: 191-198

[11]Li X Q, Minor A M. Precise measurement of activation parameters for individual dislocation nucleation during *in situ* TEM tensile testing of single crystal nickel. *Scr. Mater.*, **2021**,**197**:113764

[12]Wang L H, Zhang Y, Zeng Z, Zhou H, He J, Liu P, Chen M W, Han J, Srolovitz D J, Teng J. Tracking the sliding of grain boundaries at the atomic scale. *Science*, **2022**,**375**(6586):1261

[13]Yu Y F, Cui J Z. Elastic-plastic deformation decomposition algorithm for metal clusters at the atomic scale. *Comput. Mech.*, **2021**,**67**: 567-581

[14]Guder V, Sengul S. Tensile strength and failure mechanism of *hcp* zirconium nanowires: Effect of diameter, temperature and strain rate. *Comput. Mater. Sci.*, **2020**,**177**:109551

[15]Traiviratana S, Bringab E M, Benson D J, Meyers M A. Void growth in metals: Atomistic calculations. *Acta Mater.*, **2008**, **56**(15): 3874-3886

[16]Yang Z, Huang Y H, Ma F, Sun Y J, Xu K W, Chu P K. Size-dependent deformation behavior of nanocrystalline graphene sheets. *Mater. Sci. Eng. B-Adv. Funct. Solid-State Mater.*, **2015**,**198**:95-101

[17]Ritter Y, Şopu D, Gleiter H, Albe K. Structure, stability and mechanical properties of internal interfaces in $Cu_{64}Zr_{36}$ nanoglasses studied by MD simulations. *Acta Mater.*, **2011**,**59**(17):6588-6593

[18]Tang Y Z, Bringa E M, Meyers M A. Ductile tensile failure in metals through initiation and growth of nanosized voids. *Acta Mater.*, **2012**, **60**(12):4856-4865

[19]Cheng N, Chen F, Li R, Durkan C, Wang N, Zhao J W. Correlation between the microstructure and the deformation behaviour of metallic nanowires. *Comput. Mater. Sci.*, **2019**,**168**:116-124

[20]Pang W W, Yu S Y, Lin Z J, Zhao Y Z, Yin F X. Effects of crystal orientation and temperature on the deformation mechanism and mechanical property of Cu nanowire. *Micro Nano Lett.*, **2020**,**15**(4): 261-265

[21]Yoon J, Jang Y, Kim K, Kim J, Son S, Lee Z. *In situ* tensile and fracture behavior of monolithic ultra-thin amorphous carbon in TEM. *Carbon*, **2022**,**196**:236-242

[22]Liu Z L, Yuan X M, Wang S L, Liu S, Tan H H, Jagadish C. Nanomechanical behavior of single taper-free GaAs nanowires unravelled by *in-situ* TEM mechanical testing and molecular dynamics simulation. *Mater. Sci. Eng. A-Struct. Mater. Prop. Microstruct. Process.*, **2021**, **806**:140866

[23]Song B, Loya P, Shen L L, Sui C, He L, Guo H, Guo W H, Rodrigues Marco T F, Dong P, Wang C, He X D, Ajayan P M, Lou J. Quantitative *in situ* fracture testing of tin oxide nanowires for lithium ion battery applications. *Nano Energy*, **2018**,**53**:277-285

[24]Li P T, Yang Y Q, Koval V, Luo X, Chen J X, Zhang W, Lin E E, Wang B W, Yan H X. Temperature-dependent deformation in silver-particle-covered copper nanowires by molecular dynamics simulation. *J. Materiomics*, **2022**,**8**:68-78

[25]Wang F Y, Sun W, Gao Y J, Liu Y H, Zhao J W, Sun C Q. Investigation on the most probable breaking behaviors of copper nanowires with the dependence of temperature. *Comput. Mater. Sci.*, **2013**,**67**: 182-187

[26]Liu Y H, Zhao J W. The size dependence of the mechanical properties and breaking behavior of metallic nanowires: A statistical description. *Comput. Mater. Sci.*, **2011**,**50**(4):1418-1424

[27]Wang D X, Zhao J W, Hu S, Yin X, Liang S, Liu Y H, Deng S Y. Where, and how, does a nanowire break? *Nano Lett.*, **2007**,**7**(5):1208-1212

[28]Cui Y, Toku Y, Kimura Y, Ju Y. The deformation mechanism in cold-welded gold nanowires due to dislocation emission. *Comput. Mater. Sci.*, **2021**,**188**:110214

[29]Shen K Y, Cheng N, Zhao J W, Hou J. Correlation between the breaking behavior and the initial microstructural defects of the metallic nanowires: An approach from statistical analysis. *Comput. Mater. Sci.*, **2022**,**213**:111486

[30]Niu S C, Chang X T, Zhu Z H, Qin Z W, Li J F, Jiang Y C, Wang D S, Yang C X, Gao Y, Sun S B. Low-temperature wearable strain sensor based on a silver nanowires/graphene composite with a near-zero temperature coefficient of resistance. *ACS Appl. Mater. Interfaces*, **2021**,**13**(46):55307-55318

[31]Mishin Y, Farkas D, Mehl M J, Papaconstantopoulos D A. Interatomic potentials for monoatomic metals from experimental data and *ab initio* calculations. *Phys. Rev. B*, **1999**,**59**:3393-3407

[32]Johnson R A. Relationship between defect energies and embedded-atom-method parameters. *Phys. Rev. B*, **1988**,**37**:6121

[33]Johnson R A. Alloy models with the embedded-atom method. *Phys. Rev. B*, **1989**,**39**:12554

[34]Sun Y L, Sun W, Fu Y Q, Wang F Y, Gao Y J, Zhao J W. The deformation behaviors of silver nanowires including 3D defects under tension. *Comput. Mater. Sci.*, **2013**,**79**:63-68

[35]李韧, 赵健伟, 侯进, 贺园园, 程娜. 金属纳米线中凸凹微结构对初始形变的影响. 高等学校化学学报, **2018**,**39**(3):514-520
LI R, ZHAO J W, HOU J, HE Y Y, CHENG N. Effect of the convex and the concave microstructures in the metallic nanowires on the initial deformation behavior. *Chem. J. Chinese Universities*, **2018**,**39**(3):514-520

[36]Zhao J W, Yin X, Liang S, Liu Y H, Wang D X, Deng S Y, Hou J. Ultra-large scale molecular dynamics simulation for nano-engineering. *Chem. Res. Chin. Univ.*, **2008**,**24**(3):367-370

[37]Morales J J, Rull L F, Toxvaerd S. Efficiency test of the traditonal MD and the link-cell methods, computer physics communications. *Comput. Phys. Commun.*, **1989**,**56**(2):129-134

[38]Hockney R W, Eastwood J W. Computer simulation using particles. *SIAM Rev.*, **1983**,**25**(3):425-426

[39]Wu H A. Molecular dynamics study of the mechanics of metal nanowires at finite temperature. *Eur. J. Mech. A-Solids*, **2006**,**25**(2):370-377

[40]Foiles S M, Baskes M I, Daw M S. Embedded-atom-method functions for the *fcc* metals Cu, Ag, Au, Ni, Pd, Pt, and their alloys. *Phys. Rev. B*, **1988**,**37**(17):10378

[41]Rapaport D C. *The art of molecular dynamics simulation*. 2*nd ed*. Cambridge: Cambridge University Press, **2004**.

[42]Kelchner C L, Plimpton S J, Hamilton J C. Dislocation nucleation and defect structure during surface indentation. *Phys. Rev. B*, **1998**, **58**:11085-11088

[43]Ester M, Kriegel H P, Sander J, Xu X. A density-based algorithm for discovering clusters in large spatial databases with noise. *Proceedings of the Second International Conference on Knowledge Discovery and Data Mining*. Portland: AAAI Press, **1996**:226-231

[44]Li J G, Lei X, Ding J H, Gao Z X, Wang H, Shi Y L. Surface effect on size dependent Young′s modulus of nanowires: Exponentially decreased surface elasticity model. *Mater. Lett.*, **2022**,**307**:131001

[45]So S H, Jang J H, Sung S J, Yang S J, Nam K T, Park C R. Demonstration of the nanosize effect of carbon nanomaterials on the dehydrogenation temperature of ammonia borane. *Nanoscale Adv.*, **2019**,**1**:4697-4703

[46]Cao H, Rui Z Y, Yang F Q. Mechanical properties of Cu nanowires: Effects of cross-sectional area and temperature. *Mater. Sci. Eng. A-Struct. Mater. Prop. Microstruct. Process.*, **2020**,**791**:139644

[47]Alian A R, Ju Y, Meguid S A. Comprehensive atomistic modeling of copper nanowires-based surface connectors. *Mater. Des.*, **2019**,**175**:107812

[48]赵健伟,李韧, 程娜, 侯进. 银纳米线初始结构对拉伸形变和断裂分布的影响. 中国科学: 技术科学, **2018**,**48**(2):143-153
ZHAO J W, LI R, CHENG N, HOU J. The influence of the initial structure in the silver nanowire on the deformation mechanism and the distribution of the breaking positions. *Scientia Sinica Technologica*, **2018**,**48**(2):143-153

[49]Sung P H, Wu C D, Fang T H. Effects of temperature, loading rate and nanowire length on torsional deformation and mechanical properties of aluminium nanowires investigated using molecular dynamics simulation. *J. Phys. D-Appl. Phys.*, **2012**,**45**:215303

[50]Liu Y H, Zhao J W, Wang F Y. Influence of length on shock-induced breaking behavior of copper nanowires. *Phys. Rev. B*, **2009**, **80**:115417

[51]冯端, 师昌绪, 刘治国. 材料科学导论. 北京: 化学工业出版社, **2004**.
FENG D, SHI C X, LIU Z G. *Introduction to materials science*. Beijing: Chemical Industry Press, **2004**.

[52]Sun J P, Fang L, Ma A, Jiang J H, Han Y, Chen H W, Han J. The fracture behavior of twinned Cu nanowires: A molecular dynamics simulation. *Mater. Sci. Eng. A-Struct. Mater. Prop. Microstruct. Process.*, **2015**,**634**:86-90

[53]Sainath G, Choudhary B K, Jayakumar T. Molecular dynamics simulation studies on the size dependent tensile deformation and fracture behaviour of body centred cubic iron nanowires. *Comput. Mater. Sci.*, **2015**,**104**:76-83

[54]Xie Z C, Shin J, Renner J, Prakash A, Gianola D S, Bitzek E. Origins of strengthening and failure in twinned Au nanowires: Insights from *in-situ* experiments and atomistic simulations. *Acta Mater.*, **2020**, **187**:166-175

[55]赵健伟, 李韧, 侯进, 程娜. 纳米线断裂行为的统计分布特征与初始微观结构的关系. 中国科学: 技术科学, **2018**,**48**(7):719-728
ZHAO J W, LI R, HOU J, CHENG N. Statistical analysis of the breaking behaviors of metallic nanowires and correlation with the initial microstructure. *Scientia Sinica Technologica*, **2018**, **48**(7): 719-728